

A Sharper View of Impact Craters from Clementine Data

C. M. Pieters,* M. I. Staid, E. M. Fischer, S. Tompkins, G. He

The ultraviolet-visible camera on the Clementine spacecraft obtained high-spatial resolution images of the moon in five spectral channels. Impact craters mapped with these multispectral images show a scale of lithologic diversity that varies with crater size and target stratigraphy. Prominent lithologic variations (feldspathic versus basaltic) occur within the south wall of Copernicus (93 kilometers in diameter) on the scale of 1 to 2 kilometers. Lithologic diversity at Tycho (85 kilometers in diameter) is less apparent at this scale, although the impact melt of these two large craters is remarkably similar in this spectral range. The lunar surface within and around the smaller crater Giordano Bruno (22 kilometers in diameter) is largely dominated by the mixing of freshly excavated material with surrounding older soils derived from a generally similar feldspathic lithology.

The Clementine spacecraft acquired digital images of the lunar surface using four co-aligned framing cameras sensitive to radiation from the visible to mid-infrared (1). Preliminary results derived from processed data acquired with the ultraviolet-visible (UVVIS) camera are presented here for several impact craters on the moon. Impact cratering is a fundamental process throughout the solar system affecting all planets, including Earth. Evaluation of the composition and distribution of materials associated with craters provides important information about the impact process as well as the nature and stratigraphy of the target. The geologic and geochemical properties of terrestrial craters are severely degraded by alteration processes active in the terrestrial environment over time (2); the moon, however, provides an excellent near-pristine laboratory with which to study the impact process.

The lunar images produced globally by Clementine's framing cameras are much like LANDSAT multispectral data for Earth. Both are a measure of reflected solar radiation, and both acquire data through several spectral bandpasses (filters) that were chosen to cover parts of the spectrum for which surface materials exhibit known variations. Unlike Earth, however, the moon is almost entirely an anhydrous rocky body, an environment well suited for geologic study. Clementine filters were assigned to those parts of the visible and near-infrared (NIR) spectrum that are sensitive to both variations in bulk mineralogy (principally the abundance of iron-bearing minerals) and the cumulative amount of "space weathering" the surface has experienced (alteration due to several processes active in the space environment). Bandpasses of five filters for the UVVIS camera

are superimposed on laboratory spectral reflectance measurements of lunar samples in an accompanying report (1). We use the nominal bandpass centers for this report.

Three general reflectance properties of lunar materials can be readily measured with Clementine UVVIS filters. The first is overall albedo or brightness. Materials rich in plagioclase feldspar (Al-Ca silicate) and low in mafic (iron-bearing) minerals are relatively bright (3). Also, freshly exposed materials (materials that have not been extensively exposed to space weathering processes) are bright relative to well-developed (mature) soils (3, 4). A second general property, the steepness of the continuum throughout the visible (measured by the 415/750-nm ratio), is sensitive to both the composition and the maturity of the soil (3-5). The third property, the reflectance near 1 μm relative to the reflectance in the visible (usually 750/950-nm ratio), is sensitive to the strength and character of absorptions near 1 μm (an indication of the presence of iron-bearing minerals) and the steepness of the continuum (affected by exposure to the space environment). As a result of space weathering, the absorption near 1 μm is significantly weakened and the continuum becomes steeper (redder) (3, 5). Variations of these properties for lunar materials can be seen in the lunar sample spectra presented in (1).

Several calibration and data-processing steps are required before Clementine data can be analyzed for scientific purposes. The UVVIS camera appears to respond in a systematic manner; thus, the data can be calibrated with several additive and multiplicative corrections. A combination of preflight data bounded by information from electronics operation and early in-flight data provides initial values for dark-field subtraction, probably good to 1%. Preliminary flat-field corrections were derived from preflight data and are good to approximately 3%. Both of these corrections can be

improved as in-flight data are more thoroughly analyzed and the more comprehensive preflight data are made available in a useful format. The data were acquired with 8-bit encoding, and all but about 5% of the UVVIS data were stored as compressed data by using an efficient data compression chip (1). Because data are altered with the compression algorithm used, radiometric accuracy of individual pixels of decompressed data is reduced, the amount being dependent on the particular scene. Accuracy of the color data can be largely recovered by averaging several surrounding pixels up to an 8 pixel by 8 pixel, the block size used in the compression algorithm. The effective spatial resolution of decompressed color data is thus less than the spatial resolution initially acquired by the camera. Of the data presented here, the images of Copernicus and Giordano Bruno were acquired uncompressed, whereas the images of Tycho were acquired compressed. We used averages of 4 pixel by 4 pixel blocks in our analysis of spectral characteristics. The combined effect of the sources of error in the data presented here is about 4% filter-to-filter error in relative color (6).

For evaluation of color variations within a scene, frames acquired through different filters must be registered to each other to align features. Best results for the filter-to-filter registration were obtained through a first- or second-order transform with bilinear interpolation to perform partial pixel shifts. This registration must be performed separately for each frame set (of five filters), as relative filter positions within a given set will vary. For large features, such as Copernicus and Tycho, several frame sets must be mosaicked together.

When the first lunar data were returned, it was recognized that images through the blue filter (415 nm) were substantially degraded relative to the other filters. It is thought that this degradation is most likely due to color aberrations of the lens used. When image ratios are produced with the 415-nm image, both images must be degraded to the same level (see below). The 415-nm data also exhibit the largest high- and low-frequency variations in sensitivity across the image (flat field).

The Clementine data are presented in two forms: multispectral image composites and five-color spectra of individual areas selected within the images. The multispectral image composites were prepared from two calibrated (dark- and flat-field corrected) and co-registered ratio images with color assignments being red = 750/415 nm, green = 750/950 nm or 750/1000 nm, and blue = 415/750 nm. We have used a Gaussian filter to match the characteristics of the 750- and 415-nm images before preparation of the ratio (the filter extends over a

Department of Geological Sciences, Brown University, Providence, RI 02912, USA.

*To whom correspondence should be addressed.

7 pixel by 7 pixel filter window for the 750-nm image and over a 5 pixel by 5 pixel filter window for the 415-nm image). Color composite images for the three impact craters are shown in Fig. 1. This color scheme is similar to the one used by the Galileo Solid State Imaging System for lunar and asteroid multispectral images (7). In this color representation, variations in the extended visible continuum slope are represented by red (high 750/415 nm) to blue (high 415/750 nm) variations. Variations in the 1- μm region add yellow or green tones for larger 750/950-nm values, which imply stronger 1- μm absorptions, flatter continuum slopes, or both. Thus, this color representation captures much of the spectral variation within a scene and presents it in a comprehensible format.

To acquire five-color spectra for individual areas, several additional corrections are required. First, a frame set of images containing the Apollo 16 landing site was calibrated and co-registered (orbit 295, phase angle 27°). Data values for a mature, undisturbed region of soil near the landing site (Apollo 16b) were extracted from the image set. Data from calibrated and co-registered image sets for the three craters studied here were divided by the Clementine data values for Apollo 16 and then multiplied by a correction factor to account for differences in exposure time between image sets. The resulting five-color data were then multiplied by reflectance values for a mature Apollo 16 soil measured in the laboratory (62231). Photometric corrections for bright lunar terrain (8) were applied to bring brightness levels to a standard geometry for which incidence is 30° and emer-

gence is 0°. The resulting values represent an "absolute" spectrum for the image area, calibrated with lunar samples as the standard. As noted above, however, these spectra still contain about 4% filter-to-filter errors. The locations of representative five-color spectra are shown in Fig. 2, and the spectra themselves are shown in Fig. 3.

Impact craters can be used as windows to the lunar interior. They excavate and uplift materials from depths ranging from near-surface to as much as 1/10 the crater diameter, allowing inferences to be made about pre-impact target stratigraphy. Copernicus, a prominent impact crater on the lunar nearside 93 km in diameter, is estimated to have formed 800 million years ago (9). High spatial resolution multispectral images of the crater provide information about the distribution of pre-impact target lithologies and the process by which these materials were excavated, melted, mixed, and deposited during a major impact event. The spectral properties of Copernicus have been studied extensively with Earth-based telescopes (10, 11). Earth-based NIR data of high spectral resolution have identified specific mineralogy and lithologies at Copernicus, including olivine in the central peaks, anorthositic norite along the northern walls, and glass-bearing impact melt covering the northwestern floor. The diverse rock types indicate that the crust in this region is not homogeneous with depth (10). Because of the limited spatial resolution of previous Earth-based data, the character and scale of mixing within and around such a large impact crater could not be fully assessed. The higher spatial resolution of

Clementine data clarifies the relations between different lithologies and allows geologic issues to be addressed in more detail.

Extensive large- and small-scale heterogeneity of materials excavated by the Copernicus impact is readily evident from the color composite mosaic (Fig. 1A). Impact melt (target rock melted during the impact event), previously identified with pre-Apollo imagery (12, 13) and characterized as glass-bearing with NIR spectroscopy (14), is readily mapped with Clementine multispectral imagery (intense red in Fig. 1A). The impact melt is concentrated in large sections of the floor and in small areas along ledges of the walls, demonstrating a non-uniform distribution within the crater.

Despite the production of impact melt and the huge amount of energy involved in crater formation, diverse lithic materials have remained distinct and can be observed in the heterogeneous blocks and scarps along the crater wall. Several patterns are preserved that must relate to properties of the original target material. The localized abundance of yellow and green tones along the southern wall of the crater in Fig. 1A suggests an enhanced concentration of iron-bearing minerals in this location. When evaluated with brightness information from the 750-nm image, it can be seen that the mafic-rich areas (yellow-green) are often areas with reduced brightness. Comparison of the Clementine images of Copernicus (Fig. 2A) with Earth-based full moon images reveals that the darkness of small regions observed along the southern wall are due to inherent lithologic properties and not illumination effects. The properties

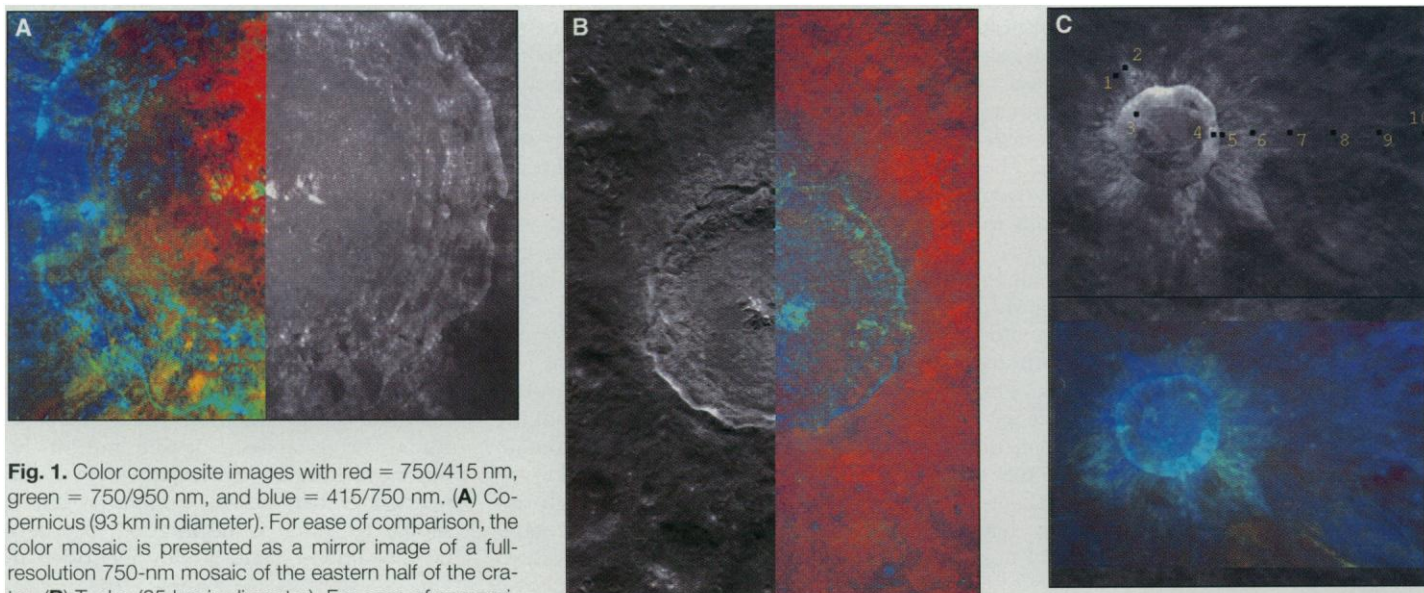


Fig. 1. Color composite images with red = 750/415 nm, green = 750/950 nm, and blue = 415/750 nm. **(A)** Copernicus (93 km in diameter). For ease of comparison, the color mosaic is presented as a mirror image of a full-resolution 750-nm mosaic of the eastern half of the crater. **(B)** Tycho (85 km in diameter). For ease of comparison, the color mosaic is presented as a mirror image of a full-resolution 750-nm mosaic of the western half of the crater. **(C)** Giordano Bruno (22 km in diameter). The image is produced from a single frame set from orbit 130; the color composite is shown below the full-resolution 750-nm

image. The numbered areas are locations for spectra shown in Fig. 3C. The uncolored portion of the color composite indicates the relative amount the 415- and 1000-nm frames were shifted to be co-registered with the 750-nm image.

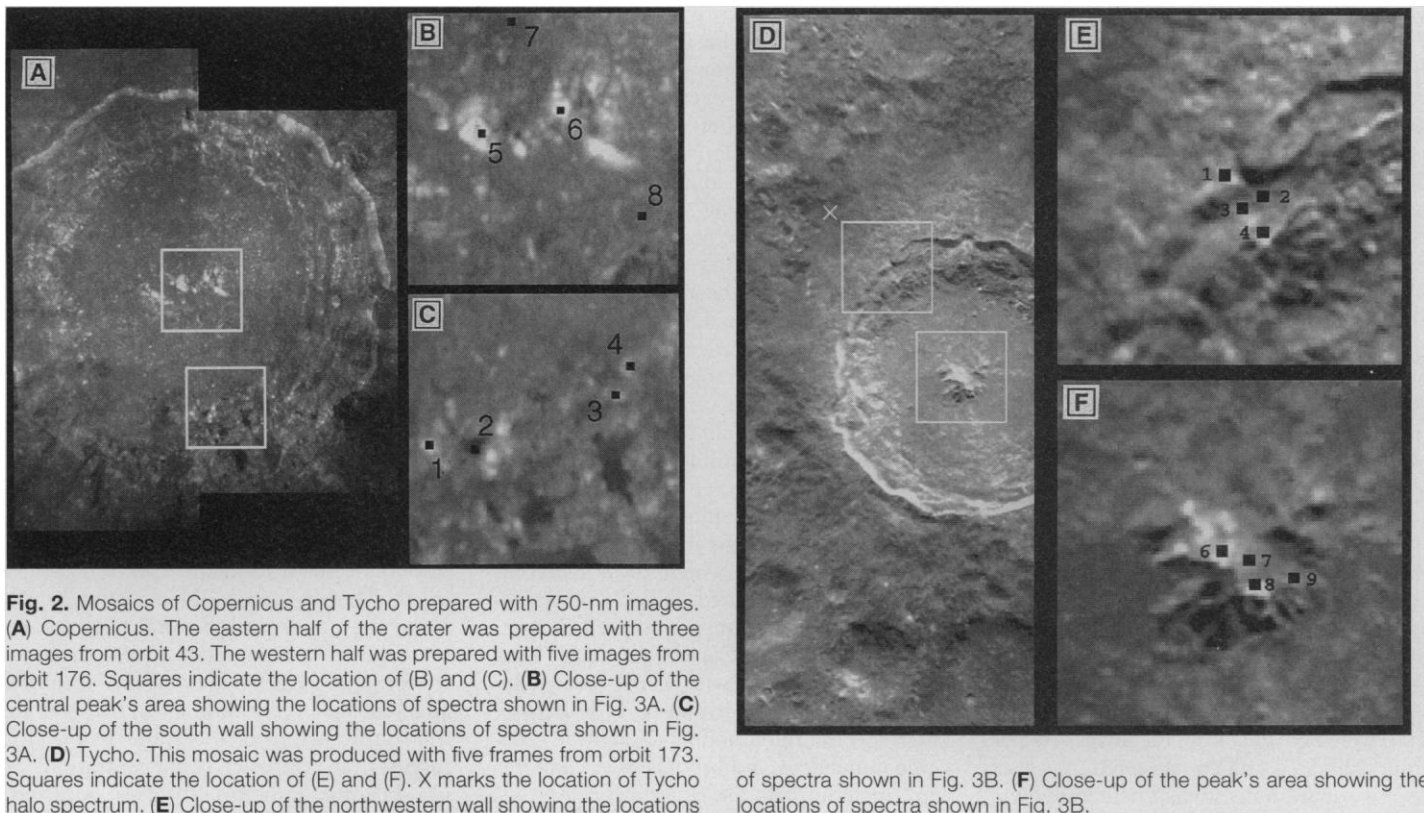


Fig. 2. Mosaics of Copernicus and Tycho prepared with 750-nm images. (A) Copernicus. The eastern half of the crater was prepared with three images from orbit 43. The western half was prepared with five images from orbit 176. Squares indicate the location of (B) and (C). (B) Close-up of the central peak's area showing the locations of spectra shown in Fig. 3A. (C) Close-up of the south wall showing the locations of spectra shown in Fig. 3A. (D) Tycho. This mosaic was produced with five frames from orbit 173. Squares indicate the location of (E) and (F). X marks the location of Tycho halo spectrum. (E) Close-up of the northwestern wall showing the

locations of spectra shown in Fig. 3B. (F) Close-up of the peak's area showing the locations of spectra shown in Fig. 3B.

of these small areas are suggestive of basaltic materials (relatively iron-rich volcanic deposits) that have been incorporated into the wall with the more common feldspathic crustal materials excavated by the crater. On the basis of stratigraphic relations derived from pre-Apollo regional imagery, the pre-impact target contained a thin layer of basalt overlying breccias derived from the Imbrium Basin to the north, which in turn overlies more ancient lunar crust (12). It can be seen that the Copernicus impact excavated these diverse materials, melted some, and produced mixtures of recognizable lithologies on the scale of 1 to 2 km. The uppermost basaltic material may have been relatively thick in the south and thin to nonexistent in the north. Broader scale spectral and compositional variations along the wall of Copernicus seen in Fig. 1A indicate that excavated and uplifted materials within the crater remained within about 30 km of their presumed origin. For example, the distinct, relatively homogeneous region along the eastern wall (blue in Fig. 1A) is 30 to 50 km from the heterogeneous (green, yellow, and blue) region comprising the southern wall, suggesting that lithologies from these two regions did not interact.

This lithologic diversity is substantiated by the five-color spectra shown in Fig. 3A. Spectra from the southern wall are indicated with solid lines. Note that two small

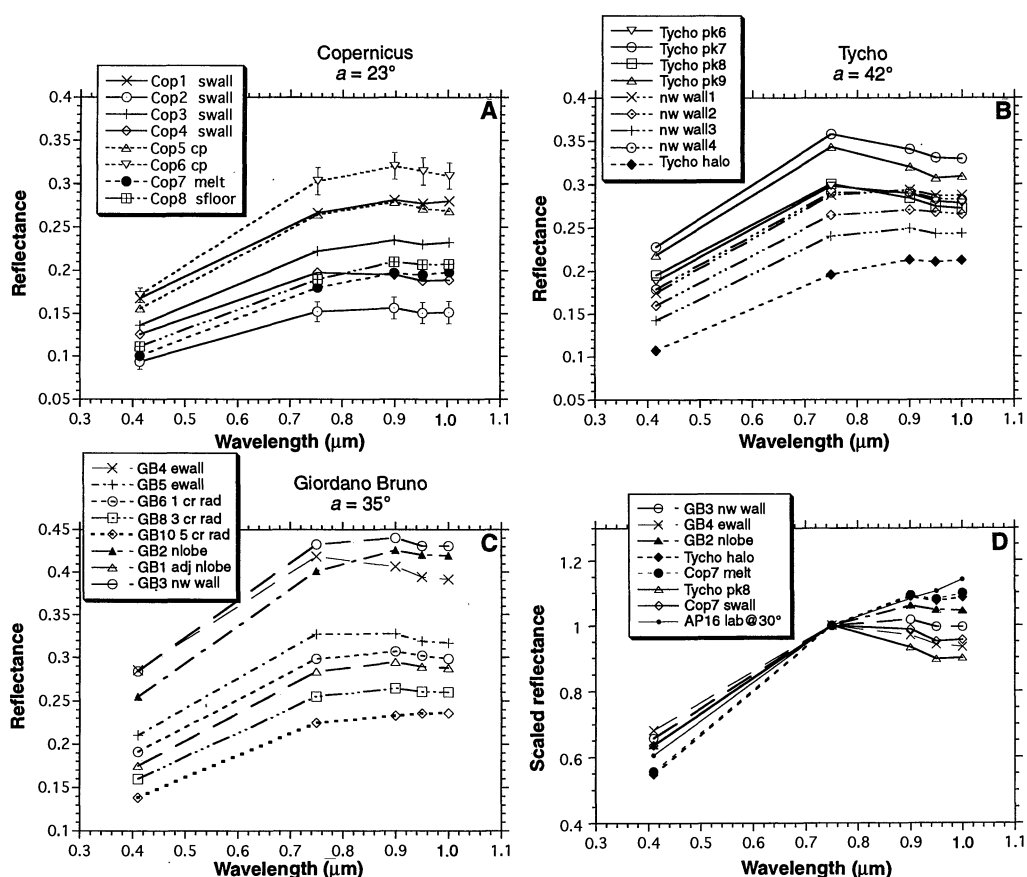
areas within the southern wall (the dark Cop2 and the intermediate Cop4) exhibit relatively strong absorption near $1\ \mu\text{m}$, consistent with blocks of excavated basalt or accumulations of mafic-rich dark mantle within the wall. Two of the central peaks (Cop5 and Cop6), known to be unusually rich in the mafic mineral olivine from Earth-based NIR spectroscopy (10), are not easily distinguished from areas within the wall that exhibit similar properties in the few spectral channels displayed in the color mosaics. On the other hand, the five-color spectra, although they cannot identify specific compositions, suggest the central peaks have either a stronger or a broader absorption near $1\ \mu\text{m}$ than do the small wall blocks (Cop1 and Cop3), allowing the peaks to be differentiated from the bright (presumably feldspathic) wall blocks.

Tycho, 85 km in diameter and formed about 100 million years ago (15), has also been surveyed with Earth-based instruments and has been identified as one of the few known highland regions to contain abundant high-calcium pyroxene and to exhibit a gabbroic lithology ($\sim 30\%$ high-calcium pyroxene) (16, 17). Tycho presents an enigma suggestive of a pluton; it is located deep within the south central highlands, yet exhibits a very uncommon composition, based on analyses of returned lunar samples and remote compositional analyses (17). Tycho also exhibits extensive impact melt,

but in contrast to Copernicus, the impact melt is located principally as a dark halo surrounding the crater (18). This halo has also been shown to contain extensive melt glass (14).

The color composite mosaic (Fig. 1B) and the five-color spectra (Fig. 3B) show that the peaks exhibit an exceptionally strong absorption near $1\ \mu\text{m}$, implying abundant mafic minerals. This reinforces the previous assessment of a distinctly gabbroic composition at Tycho (16, 17). Impact melt in the dark halo at Tycho is quite similar to that at Copernicus. The multispectral images also show remarkably sharp contacts between the mafic-rich material exposed by the impact (crater interior) and the surrounding deposits of impact melt and local highland soils. The sharpness of the contact between the interior and the exterior of the crater is particularly noteworthy. Tycho exhibits one of the most prominent ray systems on the lunar nearside, indicating that ejecta has been excavated and thrown far distances. If it were not for the impact melt, one might expect more of the near-crater deposits to exhibit properties similar to those of the interior. The dark halo of impact melt, readily identified in Fig. 2D, appears to dominate the surface properties near the crater. Although the spatial extent of these image frames (Figs. 1B and 2D) do not allow the relation between the melt halo and the surrounding

Fig. 3. Five-color reflectance spectra for the three craters discussed in this report. Error bars are typical standard deviation measurements for 4 pixel by 4 pixel blocks. As discussed in the text, additional filter-to-filter errors are approximately 4%. **(A to C)** Radiometrically calibrated spectra derived from Clementine measurements of the Apollo 16 site and an Apollo 16 soil measured in the laboratory; a is the phase angle at which the data were collected. Locations of spectra in (A) and (B) are shown in Fig. 2. **(D)** Selected spectra scaled to unity at 750 nm. A laboratory measurement of mature Apollo 16 soil (62231) is shown for comparison. Abbreviations: swall, southern wall; cp, central peak; sfloor, southern floor; pk, peak; nw wall, northwestern wall; ewall, eastern wall; cr rad, crater radius (or radii); nlobe, north lobe; adj nlobe, adjacent north lobe; lab@30°, laboratory measurement at $a = 30^\circ$.



soils to be evaluated over an extended region, at this viewing geometry (phase angle of 42°) the dark halo is indistinct from adjacent soils with these spectral bands. Tycho does not exhibit the diversity of materials within the crater as is seen at Copernicus and, although some spectral differences exist, specific variations are surprisingly small. If Tycho excavated a gabbroic pluton within the highlands, some evidence of lithologic diversity should be detected when a more thorough analysis of materials within the crater and the deposits surrounding it has been completed.

Giordano Bruno, 22 km in diameter and ≥ 800 years old (19), is substantially younger and much smaller than Copernicus and Tycho. Giordano Bruno is located in the lunar farside highlands just beyond the northeast limb. Although very fresh, it has been very poorly studied because of the limited quality of data available. The crater itself is brighter than either of the larger craters, which attests to its youth, high abundance of plagioclase, and generally low abundance of iron-bearing minerals (weak 1- μm absorption). Giordano Bruno spectra are the least red (that is, the bluest, or highest 415/750-nm ratio) of the areas analyzed here (Fig. 3D). The traverse of spectra away from the crater illustrates classic properties of fresh, relatively unweathered material mixing with an increasingly larger

fraction of preexisting weathered soils with distance. The freshest materials close to the crater are brighter, exhibit a higher 415/750-nm ratio that indicates a flatter continuum (bluer), and sometimes have more prominent features near 1 μm (and perhaps extending to longer wavelengths). The bright unusual north lobe of ejecta (GB2) may consist of shocked feldspathic material (no 1- μm feature), although it also has affinities to the impact melt spectra of the other craters (Fig. 3D). Although not analyzed quantitatively yet, it appears that along the crater wall, weathering products have already begun to accumulate down-slope (appearing redder in Fig. 1C). This observation suggests that either Giordano Bruno is substantially older than 800 years, or that the weathering process on the moon is far more rapid than currently expected.

In summary, both Copernicus and Tycho contain extensive deposits of impact melt, indicating a high-energy event capable of melting and homogenizing significant amounts of target material. The spectral properties of impact melt from these two very different, large impact craters are remarkably similar in this wavelength range. The variety of lithic materials derived from different depths, however, have not been mixed beyond recognition at either crater. A principal scale of observed lithologic

mixing at these two large craters appears to be on the order of 1 to 2 km. Copernicus exhibits substantially more heterogeneity than Tycho, which indicates a more varied stratigraphy of the pre-impact crust. In contrast to the diversity of materials observed at large impact craters which probe deep into the crust, much of the spectral variation at the smaller fresh crater Giordano Bruno is due to the varying proportion of fresh material mixed with older, more extensively exposed soil (both presumably feldspathic).

REFERENCES AND NOTES

1. S. Nozette *et al.*, *Science* **266**, 1835 (1994).
2. F. Hörz and G. S. Banholzer, *Geochim. Cosmochim. Acta* **12** (suppl.), 211 (1978); F. Hörz, R. Ostertan, D. A. Rainey, *Rev. Geophys. Space Phys.* **21**, 1667 (1983).
3. E. M. Fischer and C. M. Pieters, *Icarus*, in press.
4. J. B. Adams and T. B. McCord, *Science* **171**, 567 (1971); *Proc. Lunar Planet. Sci. Conf.* **4**, 163 (1973).
5. C. M. Pieters *et al.*, *J. Geophys. Res.* **E 98**, 17127 (1993); C. M. Pieters, E. M. Fischer, O. Rode, A. Basu, *J. Geophys. Res.* **98**, 20817 (1993).
6. Two additional sources of error affect the accuracy of the spectral calibrations but have not been incorporated into the data presented here. The first is an added signal that results from the finite (but small) amount of time required for a frame to be transferred from the imaging to storage portions of the charge-coupled device detector after exposure. The proportion of added signal varies with exposure time but could be as much as 4%. Because UVIS data were

acquired with double exposures (long and short), it is anticipated that estimated values for this readout error can be tested and improved with in-flight data. The second source of error is a more poorly defined additive signal due to scattered light. The presence of scattered light has been noted in UVVIS frames acquired for the limb of the moon (wavelength-dependent 12 to 15% at 25 pixels from the limb), but no algorithm has yet been derived for its removal. Although absolute radiance values have not been evaluated, errors would certainly be larger than the 4% estimated for relative color.

7. M. J. S. Belton *et al.*, *Science* **255**, 570 (1992); M. J. S. Belton *et al.*, *ibid.* **257**, 1647 (1992).
8. P. H. Helfenstein and J. Veverka, *Icarus* **72**, 342 (1987).
9. P. A. Eberhardt, A. Stettler, J. Geiss, N. Grosler, *Moon* **8**, 104 (1973).
10. C. M. Pieters *et al.*, *J. Geophys. Res. B* **90**, 12393 (1985); C. M. Pieters and D. E. Wilhelms, *J. Geophys. Res. C* **90**, 415 (1985).
11. P. G. Lucey, B. R. Hawke, K. Horton, *Geophys. Res. Lett.* **18**, 2133 (1991); P. C. Pinet, S. D. Chevrel, P. Martin, *Science* **260**, 797 (1993).
12. H. H. Schmitt, N. J. Trask, E. M. Shoemaker, *U.S. Geol. Surv. Misc. Map I-515* (1967); K. A. Howard, *U.S. Geol. Surv. Misc. Map I-840* (1975).
13. B. R. Hawke and J. W. Head, in *Impact and Explosion Cratering*, D. J. Roddy *et al.*, Eds. (Pergamon, New York, 1977), pp. 815–841.
14. S. Smrekar and C. M. Pieters, *Icarus* **63**, 442 (1985).
15. R. J. Drozdz *et al.*, *Proc. Lunar Planet. Sci. Conf.* **5**, 3027 (1974); R. Arvidson *et al.*, *ibid.* **7**, 2817 (1976).
16. B. R. Hawke, P. G. Lucey, J. F. Bell, *Lunar Planet. Sci. XVII*, 999 (1986).
17. C. M. Pieters, in *Remote Geochemical Analysis*, C. M. Pieters and P. Englert, Eds. (Univ. of Cambridge Press, Cambridge, 1993), pp. 309–339.
18. H. A. Pohn, *U.S. Geol. Surv. Misc. Map I-73* (1972); B. R. Hawke, D. MacLaskey, T. B. McCord, *Conf. Lunar Highlands Crust*, LPI contribution number 394, 50 (abstr.) (1979).
19. J. B. Hartung, *Meteoritics* **11**, 187 (1976).
20. We thank the group of dedicated engineers and support people at the Naval Research Laboratory, Lawrence Livermore National Laboratory, Ballistic Missile Defense Organization, and National Aeronautics and Space Administration (NASA) who brought the Clementine spacecraft and its integrated instruments safely to the moon and followed it through 2 months of very intensive operation. We are most appreciative of the NASA support for the science team involved in the data validation and scientific assessment of the data produced. We thank the two anonymous reviewers for their helpful comments.

2 August 1994; accepted 1 November 1994

Ancient Multiring Basins on the Moon Revealed by Clementine Laser Altimetry

Paul D. Spudis, Robert A. Reisse, Jeffrey J. Gillis

Analysis of laser altimetry data from Clementine has confirmed and extended our knowledge of nearly obliterated multiring basins on the moon. These basins were formed during the early bombardment phase of lunar history, have been filled to varying degrees by mare lavas and regional ejecta blankets, and have been degraded by the superposition of large impact craters. The Mendel-Rydberg Basin, a degraded three-ring feature over 600 kilometers in diameter on the lunar western limb, is about 6 kilometers deep from rim to floor, only slightly less deep than the nearby younger and much better preserved Orientale Basin (8 kilometers deep). The South Pole–Aitken Basin, the oldest discernible impact feature on the moon, is revealed as a basin 2500 kilometers in diameter with an average depth of more than 13 kilometers, rim crest to floor. This feature is the largest, deepest impact crater yet discovered in the solar system. Several additional depressions seen in the data may represent previously unmapped ancient impact basins.

Multiring basins make up the basic structural, geological, and topographic framework of the lunar crust (1, 2). Over 40 basins have been recognized and mapped on the moon [see, for example, (1)], in varying states of preservation. Although there is little controversy regarding the presence and configuration of very fresh basins, such as the magnificent Orientale basin on the western limb of the moon (1), the mapping and ring detection of very degraded, nearly obliterated multiring features is controversial (3). Controversy attends both the question of a given degraded basin's existence (3) and, if existence is granted, its size and the configuration of its rings (2–5). Until

now, such ancient features have been delineated largely through photogeologic mapping (1, 2). Altimetric data from Clementine provide a means to test both the presence and configuration of ancient basins on the moon.

The laser altimetry experiment of the Clementine mission is described elsewhere (6, 7). The data consist of points of elevation along the spacecraft orbital track (roughly, lines of longitude); each orbital ground track is separated by 2.5° at the equator, the amount of moon rotation per spacecraft revolution. The laser return detector accepted as many as four returns for each transmitted pulse, resulting in considerable noise and false returns. The distribution of real returns along an orbital track is variable, depending on terrain and solar phase angle. Real data make up as little as

15% of the total returns from the laser pulsing in very rough terrain near 0° solar phase angle but may be nearly 100% of the returns for smooth maria overflowed late in the mission, when solar phase angles were larger. However, the distribution of real returns along ground tracks is more or less continuous at crosstrack scales (~100 km), permitting the topographic point data to be gridded, binned, and contoured into a global topographic map (6, 7). This map has a surface resolution of about 200 km, adequate for the study of the global figure, regional topography, and the configuration of the largest lunar landforms, multiring basins.

The Mendel-Rydberg Basin [discovered by Hartmann and Kuiper (5); named by Wilhelms *et al.* (9)] is typical of ancient, degraded basins (1, 5, 8, 9). The basin, located on the western limb of the moon just south of the fresh, well-preserved Orientale Basin, is buried by ejecta from that structure (Figs. 1 and 2) and displays three rings measuring 630 (rim), 460, and 200 km in diameter (1). The laser profile of Mendel-Rydberg (Fig. 1) clearly shows the basin depression, averaging about 5 to 6 km in depth; inflections in the relief profile are coincident with the rings mapped by photogeology (1). Mendel-Rydberg appears to be at least partly filled by mare lavas (dark region in basin center; Fig. 1), most of which are buried by Orientale ejecta (Figs. 1 and 2); such ancient maria are widespread on the western limb of the moon (10–12). Analysis of gravity information in this region (7) indicates that a nearly flat free-air anomaly and a large positive Bouguer anomaly are coincident with the mapped position of the basin, suggesting that dense rocks, probably the mantle, are uplifted close to the surface in this region of the moon. Thus, the basin's presence is indicated not only by photogeologic and topographic information but by compositional and geophysical data as well.

Another highly degraded feature is the Coulomb-Sarton Basin [discovered by Hartmann and Wood (8); named by Lucchitta (13)], located on the northwestern portion of the lunar far side (Fig. 3) (1, 8). This basin is difficult to see on Lunar Orbiter images; it was thought to display three rings measuring 530, 400, and 180 km in diameter (Fig. 3) (1). Clementine altimetry reveals a basin about 500 km in diameter, averaging 6 km in depth, rim to floor (Fig. 3). Although the main basin rim is clearly evident, inner rings are weakly expressed; a single inner ring is visible at a diameter of about 200 km (Fig. 3). According to Wilhelms (1), the diameter of the rim of Coulomb-Sarton is uncertain, and he thought that the 400-km ring could be the basin topographic rim. The best evidence from Clementine altimetry suggests that the basin consists of two

P. D. Spudis and J. J. Gillis, Lunar and Planetary Institute, 3600 Bay Area Boulevard, Houston, TX 77058, USA.
R. A. Reisse, Science Inquiries, 312 Patteigh Road, Catonsville, MD 21228, USA.